Electrochimica Acta 513 (2025) 145610

Contents lists available at ScienceDirect

Electrochimica Acta

journal homepage: www.journals.elsevier.com/electrochimica-acta

Correlated barrier hopping dynamics of Na^+ ions in poly(vinyl alcohol) biopolymer-based solid polymer electrolytes: Electrical and structural analysis

Jacky Yong [a], Yung-Chung Chen [b], Shujahadeen B. Aziz [c], Mayeen Uddin Khandaker [d,e], Haw Jiunn Woo [a,*]

[a] Department of Physics, Faculty of Science, Centre for Ionics University of Malaya, University of Malaya, Kuala Lumpur 50603, Malaysia
[b] Department of Chemical and Materials Engineering, National Kaohsiung University of Science and Technology, Kaohsiung 807618, Taiwan
[c] Research and Development Center, Kurdistan Regional Government, University of Sulaimani, Qlyasan Street, Sulaymaniyah 46001, Iraq
[d] Applied Physics and Radiation Technologies Group, CCDCU, School of Engineering and Technology, Sunway University, Bandar Sunway, Selangor 47500, Malaysia
[e] Department of Physics, College of Science, Korea University, 145 Anam-ro, Seongbuk-gu, Seoul 02841, South Korea

ARTICLE INFO

Keywords:
Solid polymer electrolyte
Poly(vinyl) alcohol
Sodium hexafluorophosphate
Electrical properties
Conduction mechanism

ABSTRACT

In recent years, the use of sodium-ion based solid polymer electrolyte (SPE) in energy storage applications has been attracting attention in research. However, SPEs are still suffering from lower ionic conductivity in room temperature, and sodium-ion based SPEs are not yet on par with lithium-ion based SPEs in terms of the overall performance. Therefore, understanding the conduction mechanism of a sodium-ion based SPE is crucial to design and optimize the performance of a sodium-ion based device. Herein, partially hydrolyzed PVA-based SPE was prepared with $NaPF_6$. From the power law region of the plotted AC conductivity graph, the frequency exponent value, s is calculated to be $s < 1$. The decreasing of s value when temperature increases also suggests that the SPE system follows the Correlated Barrier Hopping (CBH) model where ions conduct through correlated hopping between sites by overcoming barrier heights or potential wells, with conductivity being dependent on both temperature and frequency. The SPE with PVA:$NaPF_6$ ratio of 60:40 (PVA60) exhibits the highest room temperature ionic conductivity of 3.65×10^{-5} S/cm, and has the lowest calculated activation energy of 0.149 eV. FTIR spectra confirmed the complexation of PVA and $NaPF_6$ at certain functional groups, and deconvolution at the 800–900 cm^{-1} region was done to find out the free-ions and ion-pairs percentage. The degree of crystallinity is also determined from the XRD data where PVA60 exhibits the lowest degree of crystallinity. The TGA and LSV results are also analyzed to provide an overall insight into the thermal and electrochemical stability of the samples.

1. Introduction

In view of the scarcity of fossil fuels and global climate catastrophe, the European Union has been pushing forward an escalating goal for the development of a greener prospect of renewable energy, which is said to be intermittent but unlimited. However, this conventional fuel shift to renewable energy requires a pairing with an efficient energy storage systems to collect the best energy output [1]. In the worldwide effort to address the issues of sustainability and long-term energy supply, various materials together with electrochemical energy storage (EES) technology have been widely studied and developed. Many advancements are now being made to meet the needs of technology, and the use of technical advances based on capacitance and electrochemical processes has gained recognition on a global scale [2].

Electrolyte is one of the main components for an EES device as it provides a channel for ionic conductivity and potential well. Recently, solid polymer electrolyte (SPE) has been developed as it is a better alternative to solve the safety concerns of the traditional liquid electrolyte [3]. SPE is a viable option for EES devices due to its properties in terms of compatibility, flexibility, mechanical strength, and safety [4,5]. However, SPE is reported to have low ionic conductivity compared to liquid electrolytes, which is a recurring problem for the advancement of SPE. Thus, understanding the conduction mechanism of an SPE is essential in optimizing and improving the efficiency and performance of

* Corresponding author.
E-mail address: woohj@um.edu.my (H.J. Woo).

https://doi.org/10.1016/j.electacta.2024.145610
Received 14 October 2024; Received in revised form 29 November 2024; Accepted 28 December 2024
Available online 29 December 2024

Table 1
The designation and composition of the PVA-based SPE.

Sample	Weight Ratio (PVA:$NaPF_6$)	PVA (g)	$NaPF_6$ (g)
PVA90	90:10	0.9	0.1
PVA80	80:20	0.8	0.2
PVA70	70:30	0.7	0.3
PVA60	60:40	0.6	0.4
PVA50	50:50	0.5	0.5

the electrolyte. The movement of ions (either cations or anions) through the electrolyte's polymer matrix is referred to as the conduction mechanism. SPEs require ions to pass through a polymer network, in contrast to traditional liquid electrolytes where ions travel freely in a solvent. In this work, the focus is to determine the conduction mechanism model of PVA-based SPE with sodium salt because of the lack of information on this topic in the previous literature. Various conduction models will be compared to explain the suitable mechanism of the system for this work. There are several theoretical hopping models that were proposed previously: (i) correlated barrier hopping model (CBH) model [6], (ii) quantum-mechanical tunneling (QMT) model [7], (iii) overlapping-large polaron tunneling (OLPT) model [8], and (iv) small polaron hopping (SPH) model [9].Poly(vinyl) alcohol or PVA is one of the polymers with a good potential because of its unique structural composition, which makes it a great candidate for SPE host polymer. There are two classifications of PVA based on the synthesis process: partially hydrolyzed PVA, and fully hydrolyzed PVA. In this work, note that the PVA used is the partially hydrolyzed PVA to ensure a better dissolution in the solvent. PVA is an ideal host material for SPEs because of its carbon chain backbone and hydroxyl (O–H) groups, which can act as a source of hydrogen bonding and aid in the formation of polymer complexes as well as the complexation with salt, plasticizer, and nanofiller [10,11]. Other than that, PVA also inherits some fascinating properties and advantages such as non-toxicity, high mechanical strength, biodegradability, biocompatibility, simplicity of preparation, availability, environment-friendly, cost-efficient [12].

Sodium salts are becoming a more viable option than lithium salts for energy storage applications due to the shortage and correlated price spike of lithium raw materials [13]. In the other hand, raw materials reserves for sodium are abundant in nature and generally obtainable with ease compared to lithium, leading to a cost-efficient and cheaper price of the sodium precursor like sodium carbonate, Na_2CO_3 [14]. Furthermore, as sodium-ion based devices perform better and can work in a wider temperature range, they are considered to be safer [15]. $NaPF_6$ is widely utilized as a salt in sodium-ion batteries that employ liquid organic electrolytes. This is mostly attributed to its exceptional overall characteristics, including its notable solubility in organic solvents, high anodic electrochemical stability, and resistance to corrosion in the high potential region [16]. Herein, in this work, a sodium-ion based SPE will be synthesized with materials composed of PVA as host polymer and $NaPF_6$ as salt. The combination of this polymer and salt SPE system is chosen due to their availability, cost efficiency, easy preparation, and water solubility [12–14]. Other than that, this PVA-based SPE system also aligns with the sustainability goal as PVA is biodegradable and non-toxic, rendering it an environmentally sustainable option for SPEs [15]. Additionally, sodium salts are less toxic than lithium salts. PVA also provides flexible matrix that supports the dissolution and dissociation of sodium salts. Due to the hydroxyl (-OH) groups, PVA is considered hydrophilic and making it an excellent host for ionic species like sodium ions (Na^+). Moreover, this combination of PVA and $NaPF_6$ is beneficial in terms of the novelty as no previous study has reported the performance especially the conduction mechanism of the system.

2. Experimental

2.1. Materials

The polymer host - poly(vinyl) alcohol, (PVA, 80 % hydrolyzed, molecular weight = 9000–10,000, density = 1.19–1.31 g/cm^3) was obtained from Sigma-Aldrich, and the salt - sodium hexafluorophosphate, ($NaPF_6$, 98 %, molecular weight = 167.95, density = 2.369 g/mL at 25 °C) was obtained from Macklin Chemicals. Distilled water was used as the solvent throughout the experiment.

2.2. Preparation of solid polymer electrolyte (SPE)

The technique to prepare the PVA-based SPE in this work is via solution casting method. The weight ratio of partially hydrolyzed PVA and $NaPF_6$ was varied, which the concentration of salt is increased in order to get the best conducting SPE. The composition of the PVA-based SPE and their abbreviation are summarized in Table 1. PVA was added into 20 ml distilled water with constant stirring for 2 h at room temperature. After the PVA was dissolved completely, $NaPF_6$ salt was then added into the mixture and continuously stirred at room temperature until the salt dissolved. Then, the solution was poured into a glass petri dish. Teflon foils were placed inside the glass petri dish beforehand to avoid the mixture from sticking. The solution was then placed inside an oven at 40 °C, and left for days to dry. The free standing SPE thin film was obtained after drying and the samples are kept inside a desiccator. Then, the samples were proceeded to the characterization processes.

2.3. Characterization of solid polymer electrolyte (SPE)

Electrochemical impedance spectroscopy (EIS) was performed for the conductivity studies for this work. EIS was done using the HIOKI 3532-50 LCR HiTESTER impedance analyzer at room temperature. The analyzer was paired with the BUCHI Glass Oven B-585 for conductivity analysis at various increasing temperatures. The measurements of SPEs' temperature-dependent ionic conductivity were also conducted at 10°C intervals between 30 and 80 °C. The SPE thin film was sandwiched between two blocking electrodes made of stainless steel, and the frequency range for the EIS analysis was set from 50 Hz to 5 MHz. The ionic conductivity from the EIS analysis can be determined using Eq. (1) as shown below,

$$\sigma = \frac{l}{R_b A} \tag{1}$$

where l is the sample thickness in cm, R_b is bulk resistance obtained from the Nyquist plot, and A is the surface area in cm^2 of the block electrodes.

The interaction between the polymer host, PVA and the salt, $NaPF_6$ was observed using Fourier Transform Infrared Spectroscopy (FTIR). The FTIR analysis was performed using the Thermo Scientific Nicolet™ Summit FTIR spectrometer in the range of 500–4000 cm^{-1} with a resolution of 1 cm^{-1}. The structure of the SPE samples were further analyzed with X-ray Powder Diffraction (XRD) spectroscopy using Malvern Panalytical EMPYREAN X–ray diffraction System in a 2θ angle from 5° to 80°. Thermogravimetric Analysis (TGA) was also performed using Perkin Elmer Pyris Diamond TG/DTA to analyze the thermal stability of the SPE samples, where the sample was heated from 30°C to 900 °C with heating rate of 10°C/min. The purge gas used for this TGA equipment is purified nitrogen. For the Linear Sweep Voltammetry (LSV) Analysis, it was performed using the Metrohm Autolab equipment by sandwiching the SPE between two stainless steels with the voltage range of 0–2.50 V at room temperature. LSV was done to check the potential window and the electrochemical stability of the sample.

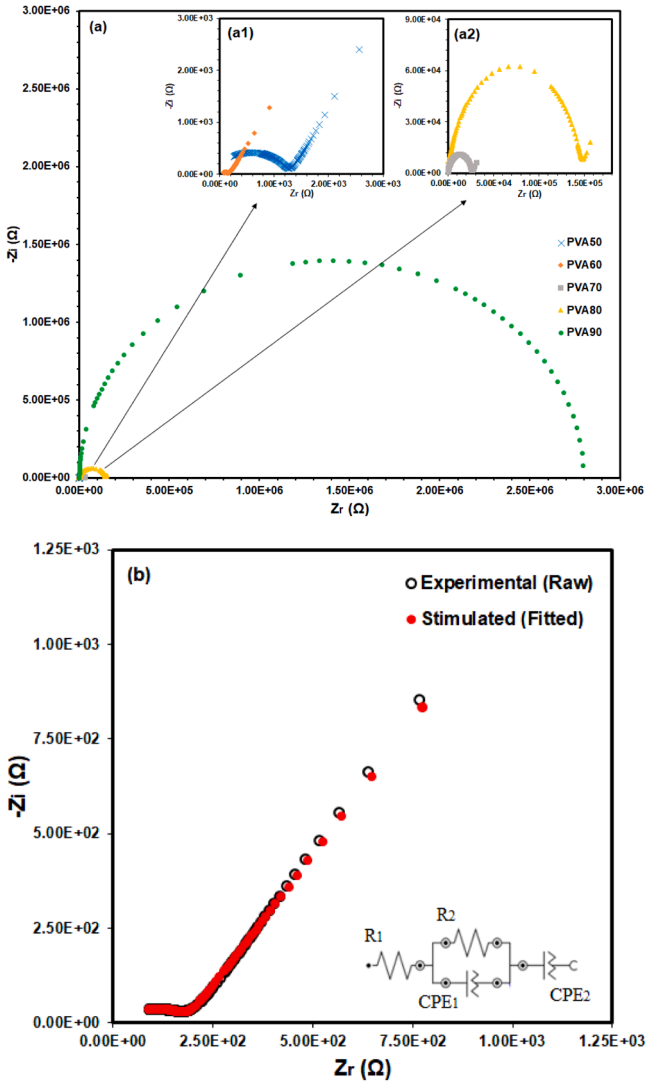

Fig. 1. Nyquist plot of (a) PVA90 with inset (a1) PVA60 and PVA50, and inset (a2) PVA80 and PVA70; Fig. 1(b) shows the experimental and fitted data with the equivalent circuit used for PVA60 at room temperature.

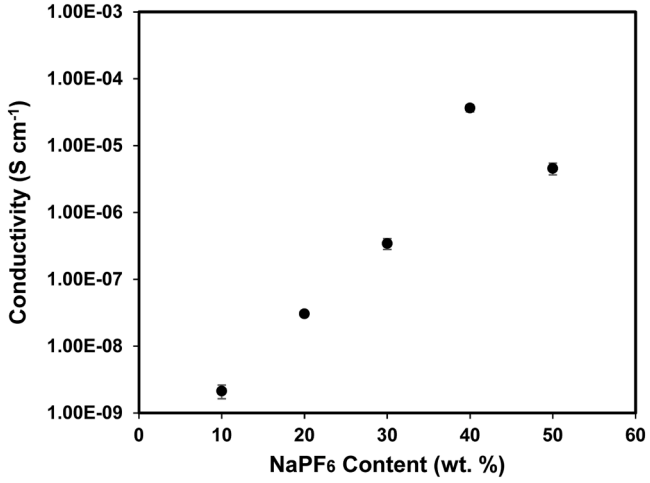

Fig. 2. The ionic conductivity of PVA-based SPE with various contents of $NaPF_6$ at room temperature.

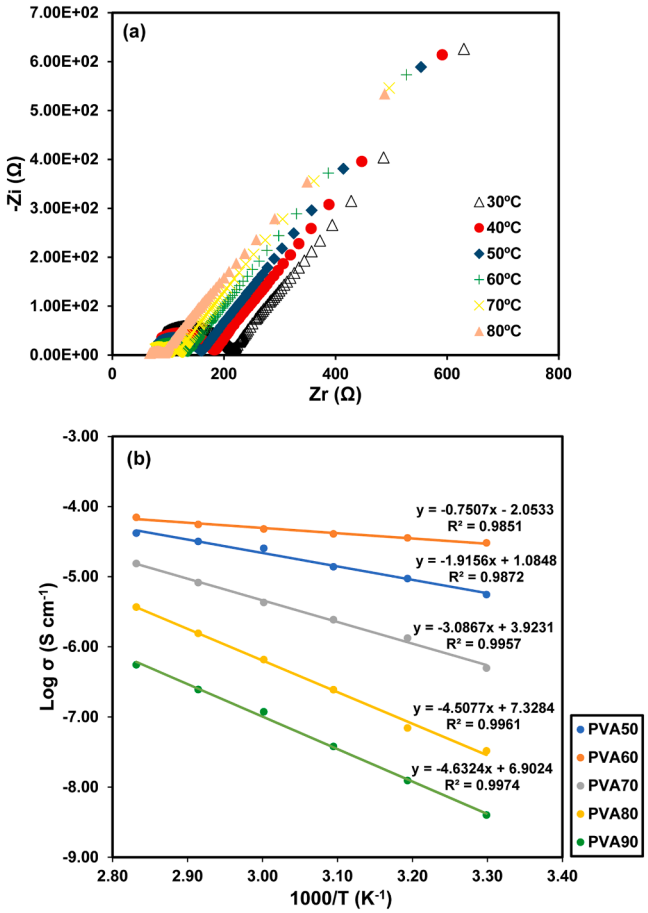

Fig. 3. (a) The Nyquist plot for PVA60 at various temperatures; (b) The Arrhenius plot of the PVA-based SPE for different $NaPF_6$ salt concentration.

3. Results and discussion

3.1. Conductivity studies

The bulk resistance (R_b) is calculated by plotting the imaginary impedance (Z_i) against the real impedance (Z_r) in a Nyquist plot. Fig. 1 (a) shows the Nyquist plot of PVA-based SPE samples with various concentrations of $NaPF_6$, and Fig. 1(f) shows the experimental and fitted data after equivalent circuit fit is applied for PVA60 at room temperature. For PVA90 in Fig. 1(a), the Nyquist plot exhibits a semicircular arc, which signifies that the sample acts as a parallel combination of a constant phase element (CPE), representing an imperfect capacitor, and a bulk resistor. The value of R_b was obtained by identifying the point of intersection between the semicircular arc and the real axis in the lower frequency range. Meanwhile, the Nyquist plot for PVA80, PVA70, PVA60, and PVA50 are characterized by a slanted spike at lower frequencies and an incomplete semicircular shape at higher frequencies. These Nyquist plots can be effectively depicted by an arrangement in series including a constant phase element (CPE) at lower frequencies and a parallel combination of a CPE and a bulk resistor at higher frequencies as shown in the illustration in Fig. 1(b). The R_b value was acquired by determining the point of intersection between the semicircular arc and the spike. All measured R_b values were compared against the fitted data, revealing consistent agreement.

The ionic conductivity was determined by employing Eq. (1) and utilizing the R_b values retrieved from the Nyquist plots. The ionic conductivity of the PVA-based SPE samples at room temperature is illustrated in Fig. 2, and it can be observed that the conductivity of the sample increases when the concentration of salt increases up to 40 wt.%.

Table 2
The activation energy calculated from the Arrhenius plot for various PVA-based SPE samples.

Designation of SPE Sample	Activation Energy, E_a (eV)
PVA90	0.919
PVA80	0.894
PVA70	0.612
PVA60	0.149
PVA50	0.380

The ionic conductivity of the SPEs demonstrated an increase at room temperature, with values increased from 2.13×10^{-9} S/cm for the PVA90 sample to 3.65×10^{-5} S/cm for the PVA60 sample. This rise was achieved by adding the $NaPF_6$ content from 10 to 40 wt.%. The observed enhancement in conductivity can be attributed to the increased number of charge carriers and the faster mobility of ions [17]. The Nyquist Plots in Fig. 1 also shows a proof of faster ion migration as the semicircle dip shifts toward the higher frequency and the bulk resistance decreases with addition of salt [18,19], which leads to an increasing ionic conductivity. However, for PVA50 with salt content of 50 wt.%, the ionic conductivity dropped. This is caused by the presence of excess ions, which cannot be effectively incorporated into the polymer matrix, leading to an increased formation of ion pairs and aggregations in comparison to the free ions [20].

3.2. Temperature dependent conductivity analysis

A study was done to analyze the temperature dependency of ionic conductivity in order to ascertain the underlying mechanism of ion transportation and the activation energy of the SPE samples. It can be observed in Fig. 3(a) and (b) that the PVA-based SPE experienced an increase in the ionic conductivity when the temperature is raised. The increasing ionic conductivity can be observed from the decreasing R_b value, where the Nyquist plot is shifting to higher frequencies as the temperature increases. The rise in conductivity is attributed to the improved flexibility of the polymer, facilitating the migration of ions between coordinating sites [21].

These SPE films also obey the Arrhenius theory. The activation energy, E_a can be calculated by using the relationship between the conductivity of the SPE samples and temperature using the Arrhenius equation as below [22]:

$$\sigma = A\, exp(-E_a / kT) \tag{2}$$

In the above expression, A represents a constant that is directly proportional to the quantity of charge carriers. $E_a$denotes the activation energy, $k$represents the Boltzmann constant, and Tsignifies the temperature measured in Kelvin units. Activation energy, commonly referred to as the minimal energy needed for charge carriers to engage in a smooth ionic migration or conduction through the electrolyte [23], typically dictates conductivity. In general, conductivity should be higher when the activation energy is lower. When a polymer system follows Arrhenius equation, the plot will be the form of a linear straight line with regression value close to unity. Fig. 3(b) shows the Arrhenius plot of the SPE samples with different $NaPF_6$ concentrations, and from the slope of the plot, the activation energy was calculated as shown in Table 2. From the plot, it is shown that the regression value is high and close to unity (~0.99) with linear plots, which confirms the system obeys the Arrhenius behavior. For the activation energy calculation from the slope, it can be observed that the activation energy for PVA60 recorded the lowest value of 0.149 eV. As mentioned in the conductivity study, PVA60 also exhibits the highest ionic conductivity. The observed decrease in activation energy can be due to the amorphousness of the SPE system, which is facilitated by the well-balanced interaction between the polymer and salt. Thus, the increase in ionic conductivity is facilitated by the thermal activation of charge carriers, wherein a faster ion migration or hopping through the bulk electrolyte occurs [24]. However, similar to the conductivity trend, the activation energy also increases at higher salt content (PVA50). The observed rise in activation energy at elevated salt concentrations can be attributed to the production of ion pairs, which subsequently leads to an increase in the viscosity of polymer chains [25]. Some of the previous studies for PVA-based polymer electrolyte have also reported that their system obeys Arrhenius behavior, including Cholant et al. for their PVA/Gum Arabic (GA) polymer system [26], Singh et al. for their PVA/imidazolium ionic liquid polymer system [27], and Saeed et al. for their PVA/NH_4NO_3 SPE system [28]. These reports explain that the decrease of activation energy for the PVA-based SPE is due to the movement of ions in the electrolyte which is promoted by the amorphous structure of the polymer film, where the increase of temperature also assist the ion hopping through the barrier.

3.3. Dielectric studies

The investigation of the relative permittivity in polymer electrolyte films contributes to the comprehension of the polarization effect occurring at the interface between the electrode and electrolyte, which additionally facilitates the establishment of a correlation between the ionic relaxation time and the conductivity [29]. The investigation of the conductivity trend can also be conducted by dielectric studies by calculating the dielectric constant (ε'), and the dielectric loss (ε") [30]. The dielectric constant is a quantitative measure of a material's polarization, which is indicative of its ability to retain or store electric charge. Additionally, it serves as a representation of the extent of dipole alignment inside a certain volume. Dielectric loss refers to the quantification of energy dissipation resulting from the movement of ions and the alignment of dipoles in response to fast reversals in the polarity of an electric field. This phenomenon is closely associated with the electrical conductivity properties exhibited by the materials involved. The dielectric constant and loss can be determined by utilizing the Eqs. (3) and (4) provided below, which involves the real and imaginary part of the complex impedance in the Nyquist plot of EIS:

$$\varepsilon' = \frac{Z''}{\omega C_o \left(Z'^2 + Z''^2\right)} \tag{3}$$

$$\varepsilon'' = \frac{Z'}{\omega C_o \left(Z'^2 + Z''^2\right)} \tag{4}$$

where C_o defined as the vacuum capacitance, which can be referred with Eq. (5):

$$C_0 = \frac{\varepsilon_0 A}{t} \tag{5}$$

where t is the thickness of the electrolyte film, A is the surface area of contact, ε_0 is the permittivity of vacuum, and ω is the angular frequency ($\omega = 2\pi f$), with f representing the frequency. Fig. 4(a) and (b) depict the dielectric constant versus *log f* plots, and the dielectric loss versus *log f* plots for PVA-based SPE incorporated with different content of $NaPF_6$ respectively.

It can be observed from Fig. 4(a) that there is high value ε' dispersion at the low frequency region. This can be attributed to the accumulation of charge carriers or dielectric polarization at the interface between the electrode and the electrolyte [29,31]. The electric field changes slowly at lower frequencies and allows for slower polarity shifts and extended relaxation time, which enables ions or dipoles to adequately migrate and accumulate at the electrode-electrolyte interface. Consequently, this results in the occurrence of electrode/electrolyte polarization. However, when operating at higher frequencies, the polarity alterations occur at a more accelerated rate, leading to a reduction in relaxation times. As a result, the charge carriers lack a sufficient amount of time to respond, resulting in a decline in the dielectric constant.

At any selected frequency, the plots of dielectric constant (ε') are

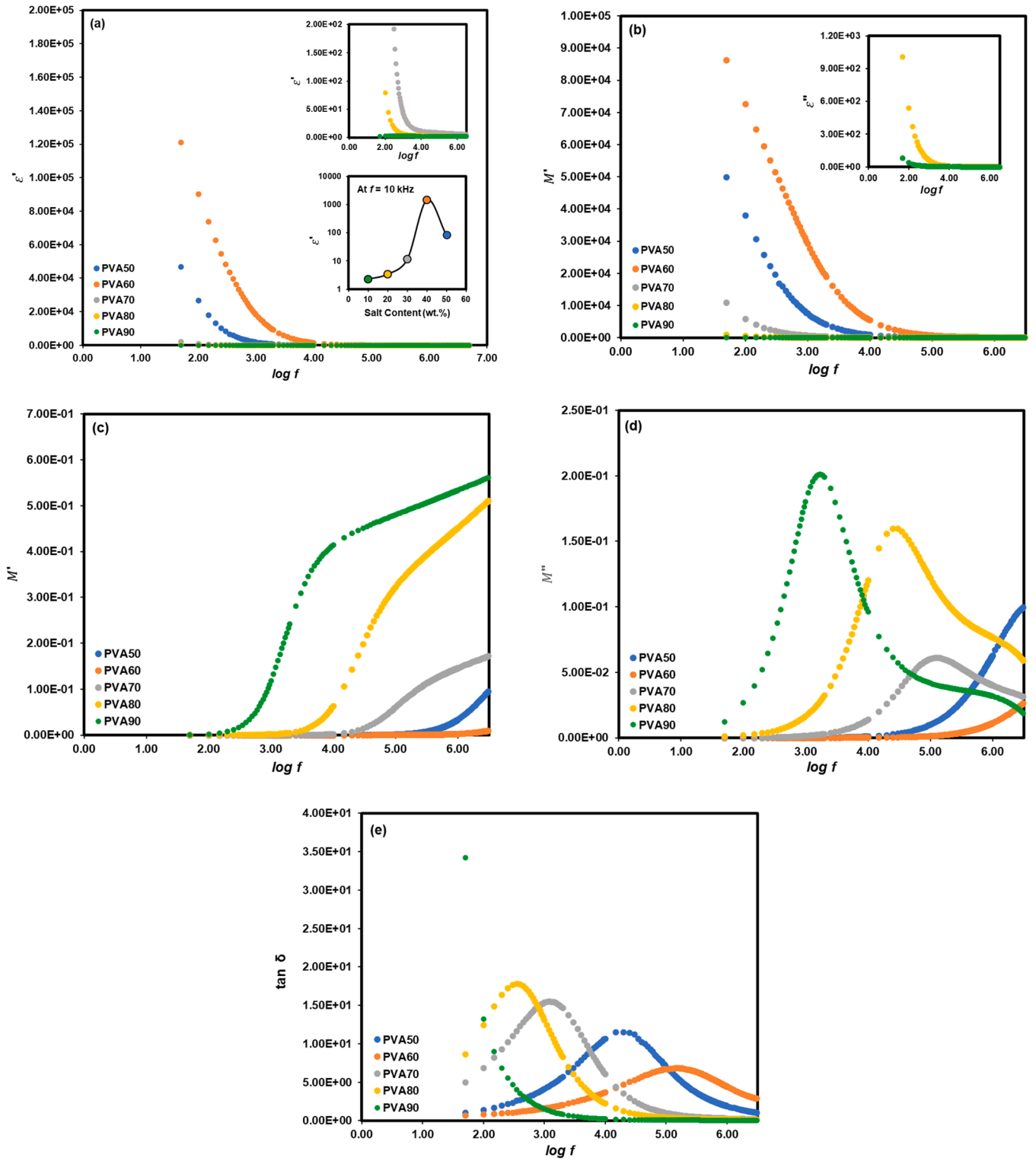

Fig. 4. The (a) ε' versus *log f* plot; (b) ε'' versus *log f* plot; (c) variation of M' versus *log f*; (d) variation of M'' versus *log f*; and (e) variation of tanδ versus *log f* of the PVA-based SPE with various concentrations of $NaPF_6$ at room temperature. The inset of Fig. 4a illustrates the zoomed part for PVA70-PVA90 (top) and the trend of ε' as a function of $NaPF_6$ content at fixed frequency, $f = 10$ kHz (bottom). The inset of Fig. 4b illustrates the zoomed part for PVA80 and PVA90.

clearly in trend with the conductivity study (an example is given in the inset of Fig. 4(a) at 10 kHz), where the highest conducting SPE sample exhibits the highest ε'. A high value of ε' typically signifies enhanced dissociation characteristics, which mitigate ion-pair formation or effectively screen the Coulombic interactions between cations and anions. According to the theory of Bjerrum, as referenced in [32,33], the critical distance r for ion-pair formation is inversely related to the ε' value, as described by the following equation:

$$r = \frac{|Z_i Z_j| e^2}{8\pi\varepsilon_0 \varepsilon' kT} \tag{6}$$

Here, Z is the valency of the cations and anions, e is the elementary

Table 3
The calculated relaxation time for various PVA-based SPE samples from the electric modulus plot.

Sample	Log f (Hz)	Frequency (Hz)	Relaxation time, τ (s)
PVA90	3.26	1800.11	8.84×10^{-5}
PVA80	4.40	24997.70	6.37×10^{-6}
PVA70	5.08	120005.18	1.33×10^{-6}
PVA60	Out of Range		
PVA50			

Table 4
The calculated relaxation time for various PVA-based SPE samples from the loss tangent plot.

Sample	*Log f* (Hz)	Frequency (Hz)	Relaxation time, τ(s)
PVA90	Out of Range		
PVA80	2.54	3.50×10^{2}	4.55×10^{-4}
PVA70	3.08	1.20×10^{3}	1.33×10^{-4}
PVA60	5.15	1.40×10^{5}	1.14×10^{-6}
PVA50	4.30	2.00×10^{4}	7.96×10^{-6}

electron charge in unit of C, ε_o is the permittivity of space, 8.85×10^{-12} F/m, k is the Boltzmann's constant 8.6173×10^{-5} eV K^{-1} and T is temperature in unit Kelvin. Ion pair formation is more likely when the interionic distance between a cation and an anion is less than r. A higher value of ε' corresponds to a reduced r, thereby decreasing the probability of ion association in systems with elevated ε', where the majority of ions remain as "free ions".

The highest value of dielectric constant achieved at PVA60 is attributed to the greater number density of charge carriers arising from the dissociation of salt inside the polymer matrix. At higher concentration of salt (PVA50), the interionic distance decreases and the Coulombic interaction between ions intensifies, resulting in the recombination of ions to create neutral ion pairs or larger clusters. This causes a drop in the number density of charge carriers, leading to a reduction in their mobility and thus diminishing their contribution to the DC conductivity [34].

Similar plots of dielectric loss (ε'') can be observed as in the variation of dielectric constant (ε'), where they both in trend with the conductivity plots. The increase of salt contents leads to an increased number density of charge carriers, resulting in higher energy dissipation. The effect reaches its peak at PVA60. The drop of dielectric loss occurs at PVA50, as a result of the re-association of ions.

3.4. Electric modulus analysis

The electric modulus in polymer electrolytes serves as a quantitative indicator of the material's capacity to store and release charge when subjected to an external electric field. It characterizes the dynamic behavior of the polymer electrolyte system in relation to variations in the frequency of the electric field, thereby offering important insights into the mechanisms governing electrical relaxation and charge transport. The relationship between electric modulus, impedance, and relative permittivity are shown in the following equations:

$$M^* = M' + jM'' = \frac{1}{\varepsilon_r^*} = \frac{1}{\varepsilon' - j\varepsilon''} = \frac{\varepsilon'}{\varepsilon'^2 + \varepsilon''^2} + j\frac{\varepsilon''}{\varepsilon'^2 + \varepsilon''^2} \quad (7)$$

$$M^* = j\omega C_0 Z^* = \omega C_0 Z'' + j\omega C_0 Z' \quad (8)$$

The electric modulus is a useful instrument for examining electrical relaxation processes since it has been defined as the reciprocal of the complex relative permittivity, as expressed by the Eq. (7). Fig. 4(c) and (d) show the electric modulus versus *log f* plots for real (M') and imaginary (M'') part, respectively.

Fig. 4(c) shows the trend of M' approaching to zero at low frequency

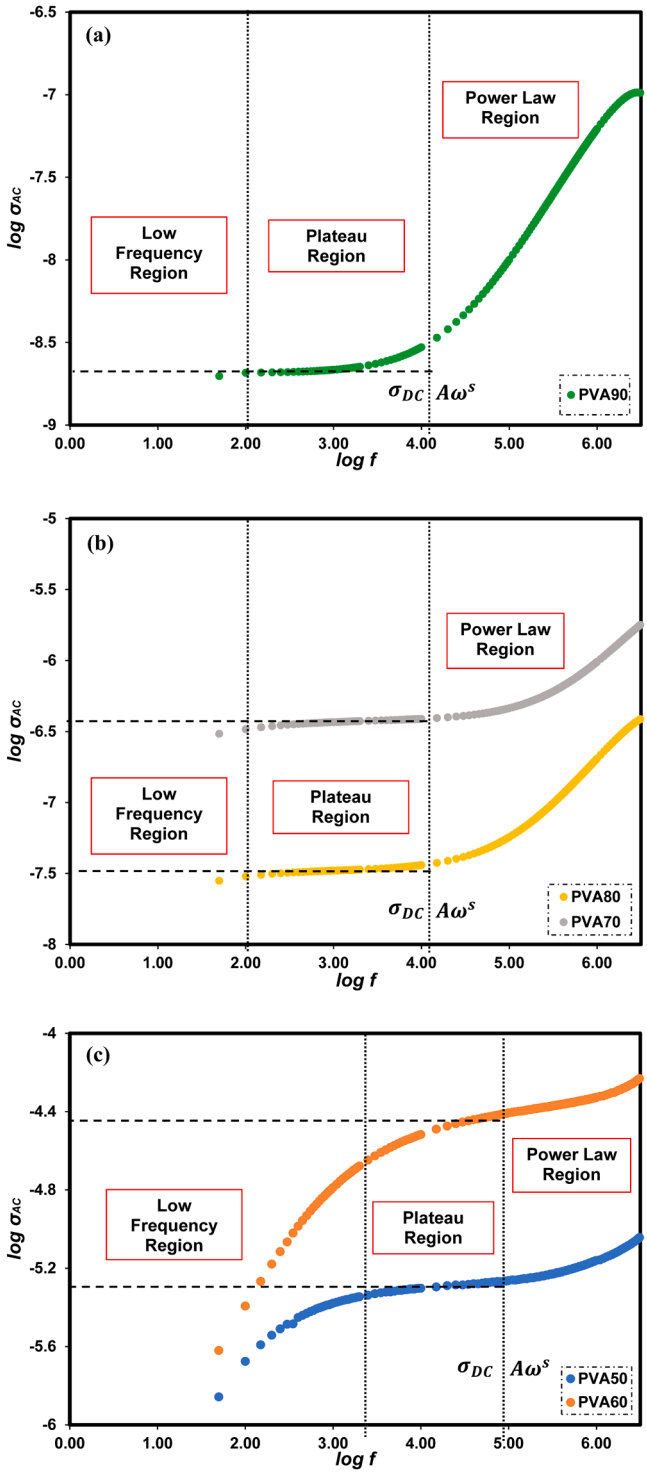

Fig. 5. The log σ_{AC} conductivity against log frequency of: (a) PVA90; (b) PVA80 and PVA70; (c) PVA60 and PVA50.

and this extended tail is attributed to the large capacitance associate with the electrode polarization. As the concentration of salt increases, the spectra display a rightward shift that extends beyond the frequency range of this particular experiment, resulting in just the dispersion component to be displayed. It is also observed that the variation of dispersion shows reverse conductivity trend. It can be observed in Fig. 4 (d) that there are broad and asymmetric peaks in the high frequency region for PVA90, PVA80, and PVA70. As salt concentration increases, the peak is observed to shift towards the higher frequencies,

Table 5
Data of estimated and calculated DC conductivity obtained log AC conductivity graph against *log f*.

Sample	Log σ AC (S/cm)	Estimated σ DC (S/cm)	Calculated σ DC (S/cm)	Percentage accuracy (%)
PVA50	-5.372	4.25×10^{-6}	4.56×10^{-6}	93.148
PVA60	-4.447	3.57×10^{-5}	3.65×10^{-5}	97.992
PVA70	-6.433	3.69×10^{-7}	3.44×10^{-7}	92.589
PVA80	-7.489	3.24×10^{-8}	3.05×10^{-8}	93.715
PVA90	-8.668	2.15×10^{-9}	2.13×10^{-9}	99.276

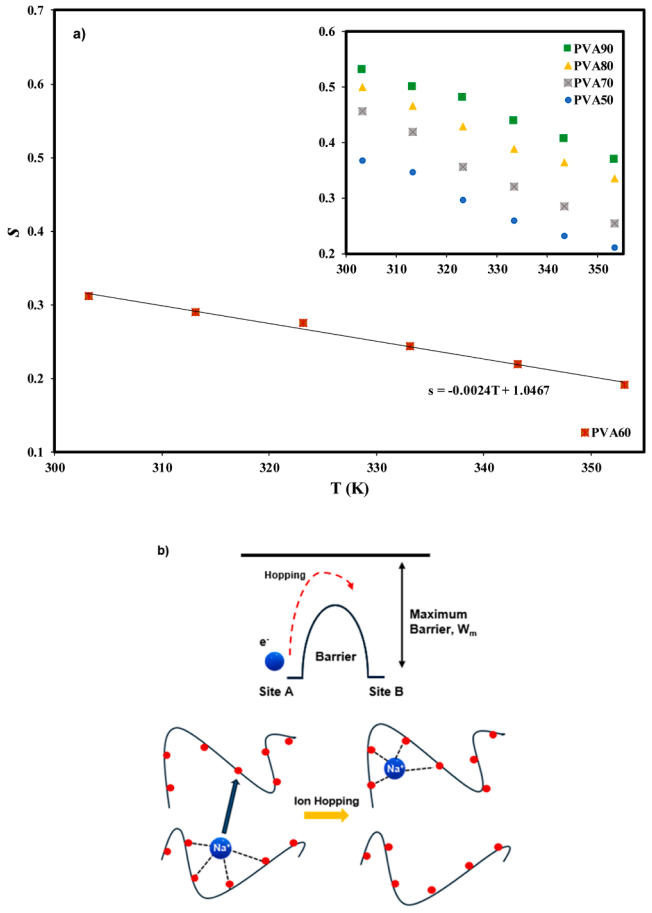

Fig. 6. (a) The frequency exponent, *s* versus temperature in Kelvin for the highest conducting sample (PVA 60). The inset shows the temperature dependence of the exponent s for PVA90, PVA80, PVA70, and PVA50. (b) The illustration of CBH model.

accompanied by a decrease in relaxation time, as anticipated. The relaxation time can be calculated using peak frequencies (f_m) with the equation below:

$$\tau = \frac{1}{2\pi f_m} \tag{9}$$

The calculated values of the relaxation time are shown in Table 3. The dispersion variation for M'' versus *log f* shows the same trend as stated previously, which means that relaxation time decreases as the conductivity increases. The relaxation time observed in the electric modulus is denoted by the conductivity relaxation time, which is due to a resonance effect that occurs when the external field is comparable to the natural frequency, resulting in maximum energy transfer.

3.5. Loss tangent analysis

The investigation of loss tangent peaks pertains to the study of the relaxation processes of SPEs. The loss tangent, denoted as tan δ, can be determined by utilizing the Eq. (10) below:

$$\tan\delta = \frac{\varepsilon''}{\varepsilon'} = \frac{Z'}{Z''} \tag{10}$$

The term "dissipation factor" is used to refer to the ratio between energy loss and energy stored. The present research examines the behavior of tanδ in polymer electrolytes to observe their relaxation properties. The plot of loss tangent as a function of frequency for PVA-based SPE with various concentrations of salt at room temperature is presented in Fig. 4(e). The loss tangent exhibits a distinct peak at a specific frequency. The shift of the loss peak towards higher frequency is evident when the salt content increases. However, PVA50 sample shifted back towards the lower frequency.

By considering the Debye equation under ideal conditions, assuming that the static dielectric constant and high frequency dielectric constant are nearly equal, the relaxation time can also be determined using Eq. (9) as shown in electric modulus analysis section. The relaxation time calculated is tabulated in Table 4. From the calculated relaxation time data, it is observed that the relaxation time variation is the inverse of the ionic conductivity value. This means that relaxation time decreases as the conductivity increases. As PVA60 exhibits the highest conductivity in this work, the relaxation time is also the lowest (1.14×10^{-6} s). The added amount of salt causes the amorphous region to expand, resulting in a loosening and weakening of molecular packing. This leads to a more flexible orientation of the polymer chain and that results in a decrease in relaxation time [35].

3.6. AC conductivity analysis and conduction mechanism

The AC conductivity can be determined by utilizing the dielectric constant (ε'), and the loss tangent (tanδ) at each frequency in accordance with the equations below:

$$\sigma_{AC} = \varepsilon_o \varepsilon' \omega \tan\delta \tag{11}$$

or

$$\sigma_{AC} = \varepsilon_o \varepsilon'' \omega \tag{12}$$

where ε'' is the dielectric loss and $\tan\delta = \frac{\varepsilon''}{\varepsilon'}$ as stated in Eq. (10). The plotted AC conductivity versus the frequency graph is represented in Fig. 5.

The AC conductivity spectra can be categorized into three main sections. The first section is in the low frequency region. This section is commonly referred to as electrode polarization (EP) effect, which can be attributed to interfacial interactions between the electrode and electrolyte [36]. In the intermediate-frequency section, there is an observable plateau in the AC conductivity that corresponds with the DC conductivity. Table 5 shows the correlation between AC conductivity and DC conductivity, where σ_{DC} can be estimated. The estimated σ_{DC} then compared with the calculated σ_{DC} in conductivity study previously. The comparisons show that the values are almost similar to each other, proving that the AC conductivity plots are valid. The high frequency region is called the dispersion region, or the power law region. As can be seen in Fig. 5, the reduction of the dispersion region is closely linked to the elimination of the high-frequency semicircle observed in the Nyquist plot due to the addition of salt. This demonstrates a strong association between impedance analysis and the dispersion of AC conductivity. The characterization of ion conduction in solid polymer electrolytes is significantly influenced by the presence of dispersion region, which the calculation of the frequency exponent (*s*) can be done. The correlation between the AC conductivity and the movement of charge carriers can be well described by Jonscher's relation:

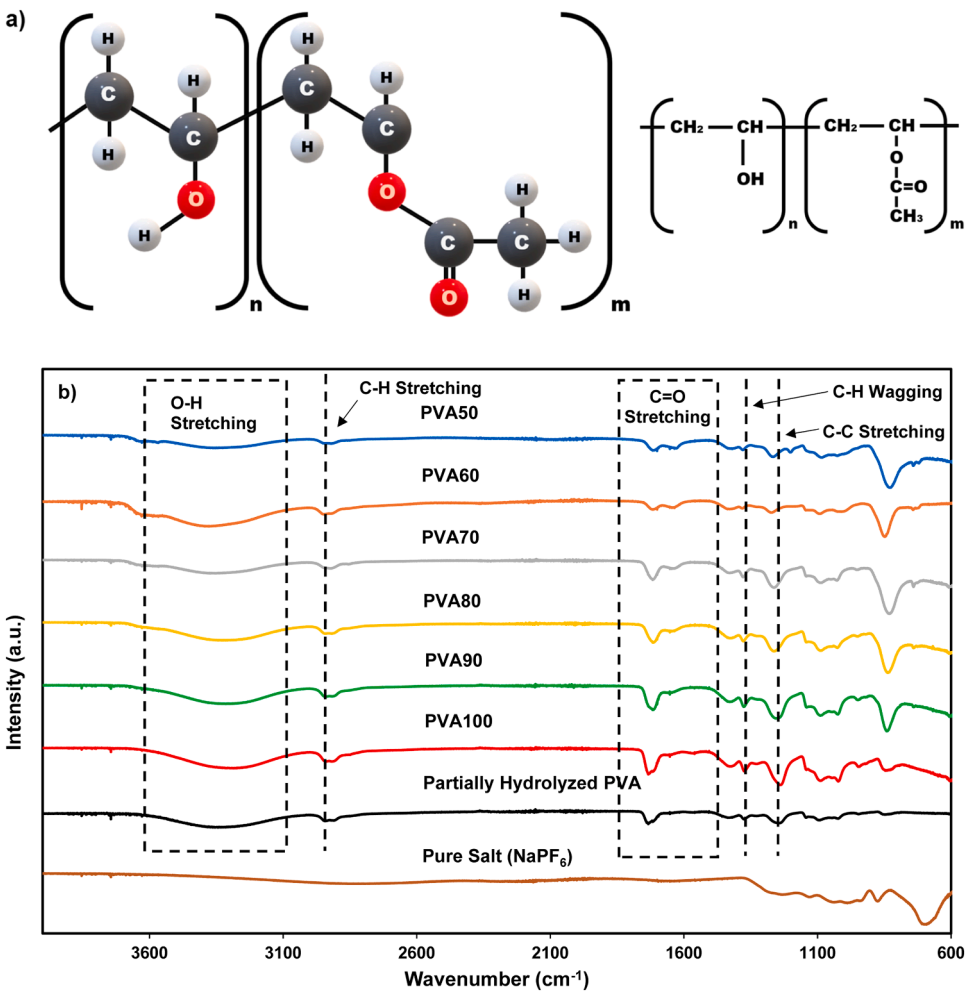

Fig. 7. (a) Illustration of the partially hydrolyzed PVA chemical structure. (b) FTIR spectra for pure salt ($NaPF_6$), partially hydrolyzed PVA, and PVA-based SPEs with various concentration of salt.

Table 6
Absorption peaks and functional group assignments of the PVA-based SPEs with various salt concentrations.

Assignment of Bands	Wavenumber (cm^{-1})							Refs.
	Pure PVA	PVA100	PVA90	PVA80	PVA70	PVA60	PVA50	
O-H stretching	3314	3285	3315	3331	3373	3377	3352	[11,40]
C-H stretching	2941	2939	2942	2943	2945	2947	2945	[11,40–42]
C=O stretching	1733	1733	1716	1715	1716	1717	1717	[41,42]
C-H bending	1419	1428	1428	1428	1428	1437	1420	[42,43]
C-H wagging	1373	1372	1375	1378	1379	1381	1380	[42,43]
C-C stretching	1238	1239	1253	1262	1262	1274	1265	[40,42,43]
C-O stretching	1090	1090	1089	1085	1090	1089	1082	[42,43]
C-H rocking	846	843	839	836	832	849	830	[42,43]

$$\sigma(\omega) = \sigma_{DC} + A\omega^s \tag{13}$$

$$\sigma_{AC} = A\omega^s \tag{14}$$

Here, we denote the total direct current (DC) and alternating current (AC) conductivity as $\sigma(\omega)$. The DC conductivity, denoted as σ_{DC}, is the component that is frequency-independent. A is a parameter that is temperature-dependent, whereas s is the exponent in the power law equation, which falls within the range of 0 to 1. The frequency exponent s can be determined from the slope of the log-log plot of the dispersion or power law region slope. This value is instrumental to determine the ion conduction mechanism. Fig. 6(a) shows the variation of s value versus the temperature in Kelvin. It can be observed that all PVA-based samples show decreasing s value when the temperature increases. Since s decreases with increasing T, it can be inferred that it adheres to the correlated barrier hopping (CBH) model as illustrated in Fig. 6(b) [6]. As shown in Fig. 6 as well, the system for PVA60 can be fitted to the equation $s = -0.0024T + 1.046$, and from this fitting equation, $s \to 1$ when $T \to 0$. For CBH model, the approximated frequence exponent s can be calculated by the following equation,

$$s = 1 - \frac{6kT}{W_m} \tag{15}$$

where W_m is referred as the maximum barrier height. From Eq. (15), it can be inferred that $s \to 1$ when $T \to 0$ as well. This further confirms the

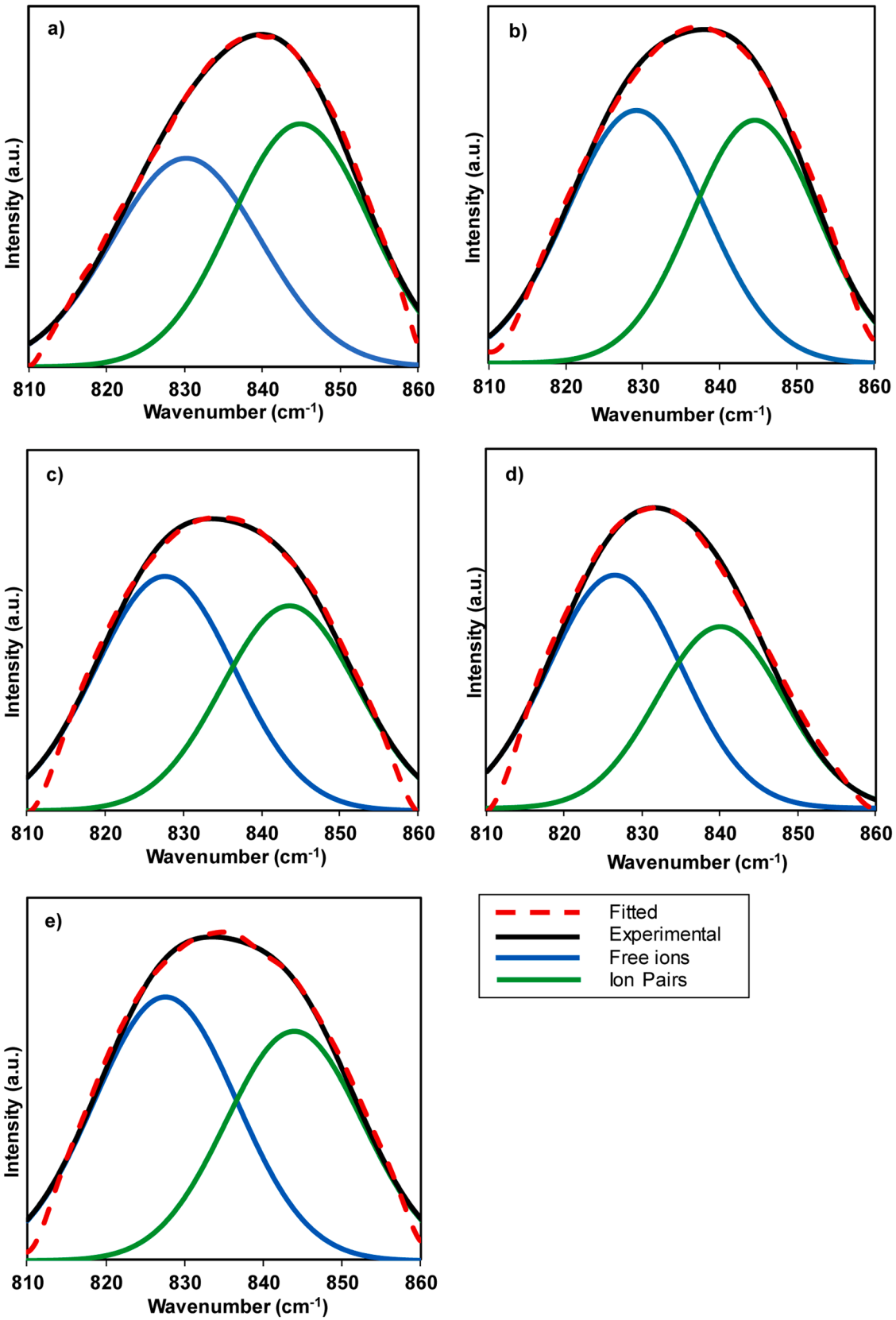

Fig. 8. Deconvolution of the PF_6^- vibration modein the region 810–860 cm^{-1} for: (a) PVA90; (b) PVA80; (c) PVA70; (d) PVA60; (e) PVA50.

Table 7
The percentage of ion species using the FTIR deconvolution method.

Designation	Salt Content (wt.%)	Free Ions (%)	Ion Pairs (%)
PVA90	10	48.12	51.88
PVA80	20	53.23	46.77
PVA70	30	54.06	45.94
PVA60	40	57.55	42.45
PVA50	50	54.52	45.48

conduction mechanism of the system follows the CBH model. In this conduction mechanism, the ions overcome the correlated energy barriers by hopping between neighbouring sites, resulting in the transport of charge through the SPEs. This model postulates that the ions or charge carriers are encompassed by several potentials, including the Coulombic repulsive potential arising from the interactions between multiple ions, as well as a potential well that accommodates the ions. The superposition of potentials results in the formation of a single-ion potential that is effectively experienced by the ion. When an ion acquires sufficient energy and transitions from one site to another, two competing relaxation processes may take place. These processes involve either a return to the initial site or the creation of a new potential barrier, resulting in an increase in the barrier height for the return transition. Consequently, the ions persist in their forward movement. According to the quantum-mechanical tunnelling (QMT) model, the *s* value is nearly equal to 0.8 and rises a little with rising temperature or independent of temperature [37]. This is why the QMT model is not applicable to this system. According to overlapping-large polaron tunnelling (OLPT) model, the *s* value is dependent on both temperature and frequency. *s* value drops with rising temperature from unity at room temperature to a lowest value at a certain temperature, then *s* value rises back with increasing temperature [37]. The *s* value for the system in this work does not follow the OLPT trend. Therefore, OLPT model does not applicable to this system. For small polaron hopping (SPH) model, it is stated that the *s* value for this model will increase when the temperature increase, and the *s* value is less than 1 [38]. This means that this work also does not follow the trend of SPH model. Since sodium-based SPEs are relatively new, the conduction mechanism of lithium-based from previous reports are reviewed. The previous research by Abdullah et al. [39] reported that a lithium-based biopolymer blend electrolyte consisting of chitosan, and methylcellulose, complexed with lithium iodide also follows the CBH conduction mechanism.

3.7. FTIR analysis

FTIR is a technique used to analyze the chemical composition of materials by detecting how they absorb infrared light. Infrared spectroscopy involves shining infrared light onto a sample and measuring how much of that light is absorbed at different wavelengths. The resulting spectrum provides information about the functional groups, chemical bonds, and molecular structure present in the sample. The chemical structure of partially hydrolyzed PVA and FTIR spectra can be observed in Fig. 7.

For FTIR, PVA100 was prepared, and it is comprised of only partially hydrolyzed PVA powder (1.0g) mixed with solvent with no addition of salt. PVA100 will be the reference spectra to be compared with the other complexed SPEs. The intermolecular hydrogen bonded O-H stretching frequency of partially hydrolyzed PVA can be observed in the region 3286 cm^{-1} for PVA100, and it shifted to 3377 cm^{-1} for PVA60. Next, the C-H stretching of CH_2 can be observed in the region 2939 cm^{-1} for PVA100, and it shifted to a higher wavenumber of 2947 cm^{-1} for PVA60. An absorption band is observed in the region 1372 cm^{-1} for PVA100 which suggests the presence of C-H wagging, and the spectra shifted to 1381 cm^{-1} for PVA60. In addition to that, a shifting also occurred at the C-C stretching spectra which the wavenumber shifted from 1239 cm^{-1} to 1274 cm^{-1} for PVA100 and PVA60 respectively. These shifts and changes

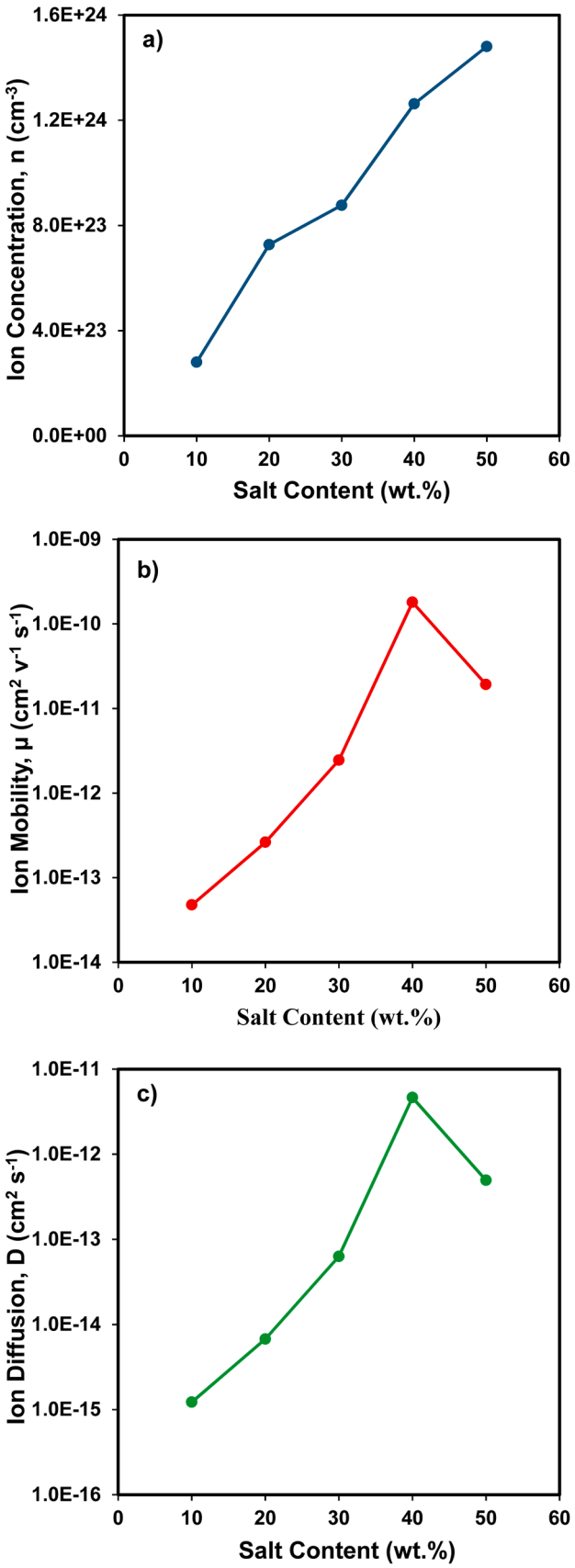

Fig. 9. The plot of: (a) ion concentration (*n*); (b) ion mobility (μ); and **c)** ion diffusion (*D*) against the $NaPF_6$ concentration added in the PVA-based SPE system.

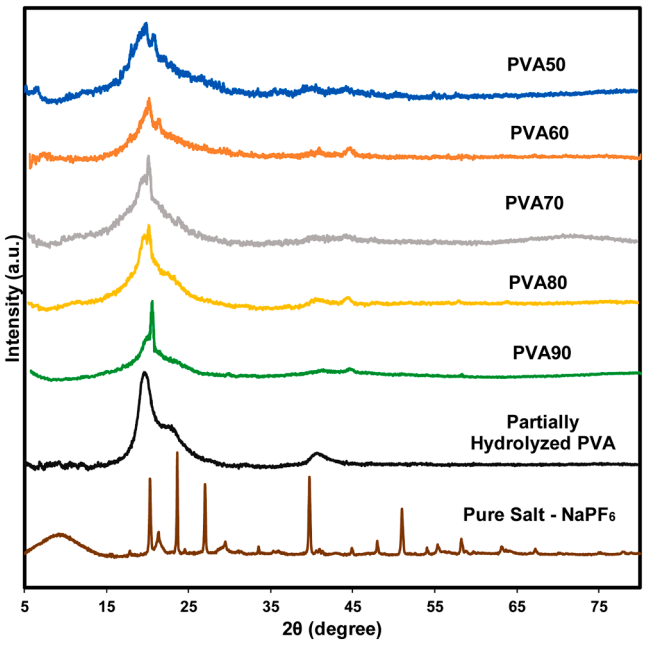

Fig. 10. The XRD result for pure $NaPF_6$, partially hydrolyzed PVA, and various samples of SPE added with different concentrations of salt.

in the FTIR spectra are clear evidence if the interaction between PVA and the sodium salt [40]. Notice that for PVA50, the absorption spectra in the region stated previously were all shifted back to a lower wavenumber. This reversal in the wavenumber shift indicates that it might be due to excessive alterations in the sample environment caused by an excessively high concentration of salt. The absorption peaks and the functional group assignments are tabulated in Table 6 with Refs. [11, 40–43].

The ion-ion interactions can only be explored by analyzing the anion peaks only as it is understood that free cations are inactive to the infrared (IR) spectrum due to their lack of distinctive absorption bands in the typical IR range. Therefore, the analysis often focuses on studying the anion peaks to extract information about ion pairs and free anions. In this research, deconvolution techniques can be applied to separate and analyze the different vibration modes within the anion's spectrum, where in this case the salt's anions are PF_6^-. This process of deconvolution helps in distinguishing the various contributing factors to the anion's absorption band, such as free anions and ion pairs. The deconvolution of the free ions (PF_6^-) and ion pairs (Na^+ - PF_6^-) is done by using Origin Pro software at the 800–900 cm^{-1} region [44,45]. The deconvolution results in two peaks, at lower wavenumber, are linked with free ions, and higher wave number is linked with ion pair. The area under the peak is associated with the fraction of free ions and ion pairs. The formulas to get the percentage for both free ions and ion pair are as below:

$$Free\ Ions\ (\%) = \frac{A_f}{A_f + A_{ip}} \times 100\% \tag{16}$$

$$Ion - Pairs\ (\%) = \frac{A_{ip}}{A_f + A_{ip}} \times 100\% \tag{17}$$

where A_f is the area of free ions, and A_{ip} is the area of ion-pairs. The conversion of transmittance to absorbance mode was performed at the 800–900 cm^{-1} region for each PVA-based SPEs spectra. The deconvoluted data can be viewed in Fig. 8, while the fraction or percentage of free ions and ion pairs can be viewed in Table 7.

Following that, by utilizing the determined percentage of free ions, the ion concentration (n), ion mobility (μ), and ion diffusion (D) can be calculated. The formulas for these three parameters are shown on Eqs. (18), (19), and (20) respectively.

$$n = \frac{M \times N_A}{V_{total}} \times (\%\ of\ Free\ ions) \tag{18}$$

$$\mu = \frac{\sigma}{ne} \tag{19}$$

$$D = \frac{\mu kT}{e} \tag{20}$$

The calculated values of the three parameters are then plotted as shown in Fig. 9. Based on the plotted result, it can be observed that the ion concentration (n) increases when more salt is added. The addition of salt will provide more charge carriers in the PVA-based SPE system [46]. In the other hand, both ion mobility (μ) and ion diffusion (D) increases from 10 wt.% (PVA90) to 40 wt.% (PVA60) but dropped when 50 wt.% of salt is added (PVA50). The increments of both parameters are due to the improvement of chain flexibility, and the decrease in parameters is a result of the collisions that occur between free ions when there is an excess of ions present [47]. Due to the limited space available, the ions experience decreased mobility and diffusivity in this form.

3.8. XRD analysis

The XRD patterns for pure $NaPF_6$, partially hydrolyzed PVA, and various SPE samples are shown in Fig. 10. Pure $NaPF_6$ displayed various peaks with high intensity at $2\theta = 20.3^o$, 21.3^o, 23.6^o, 26.9^o, 39.7^o, and 50.9^o representing its crystalline nature. . For the partially hydrolyzed PVA, crystalline peak is displayed at $2\theta = 19.7^o$, showing the typical (101) plane as well as two amorphous halos centered at 23.2^o, and 40.8^o are also depicted [48]. The degree of crystallinity of the various SPE samples can be calculated from the XRD result using the formula as follows:

$$Degree\ of\ Crystallinity\ (\%) = \frac{A_c}{A_t} \times 100\% \tag{21}$$

where A_c is the area of all the crystalline peaks, A_t is the total area of amorphous and crystalline in the XRD peaks [49]. The areas of the XRD results are deconvoluted and analyzed using the OriginPro software as shown in Fig. 11. Note that as salt is added, two crystalline peaks appeared at $2\theta = \sim 20.0^o$ and $\sim 45.0^o$ (labelled in yellow and pink line in Fig. 11, respectively). These peaks are not included in the degree of crystallinity calculation as they belong to the salt. So, only the peaks that belong to the polymer/PVA are considered in the calculation. The degree of crystallinity of the SPEs are tabulated in Table 8. The degree of crystallinity obtained is observed to be in trend with the conductivity data. This means that the addition of $NaPF_6$ is proven to increase the ionic conductivity due to the decrease of the crystalline nature of the samples.

3.9. TGA analysis

The TGA curves are shown in Fig. 12(a) and (b), which displays the weight percentage over temperature for partially hydrolyzed PVA, salt ($NaPF_6$), PVA100, PVA90, and PVA60. Similar to FTIR, PVA100 was prepared as a reference plot for the SPE samples. The small weight percentage loss observed at lower temperature for all the pure samples and SPE samples can be due to the elimination of contaminants and the evaporation of absorbed moisture during the sample preparation process. For the SPE samples (PVA100, PVA90, and PVA60), the weight loss up until 100 °C is due to the evaporation of the solvent (distilled water) and contributed by the weight loss from the decomposition of the salt itself [50].

For the $NaPF_6$ salt curve, it can be observed that the weight percentage decreases slowly and consistently as the temperature increases.

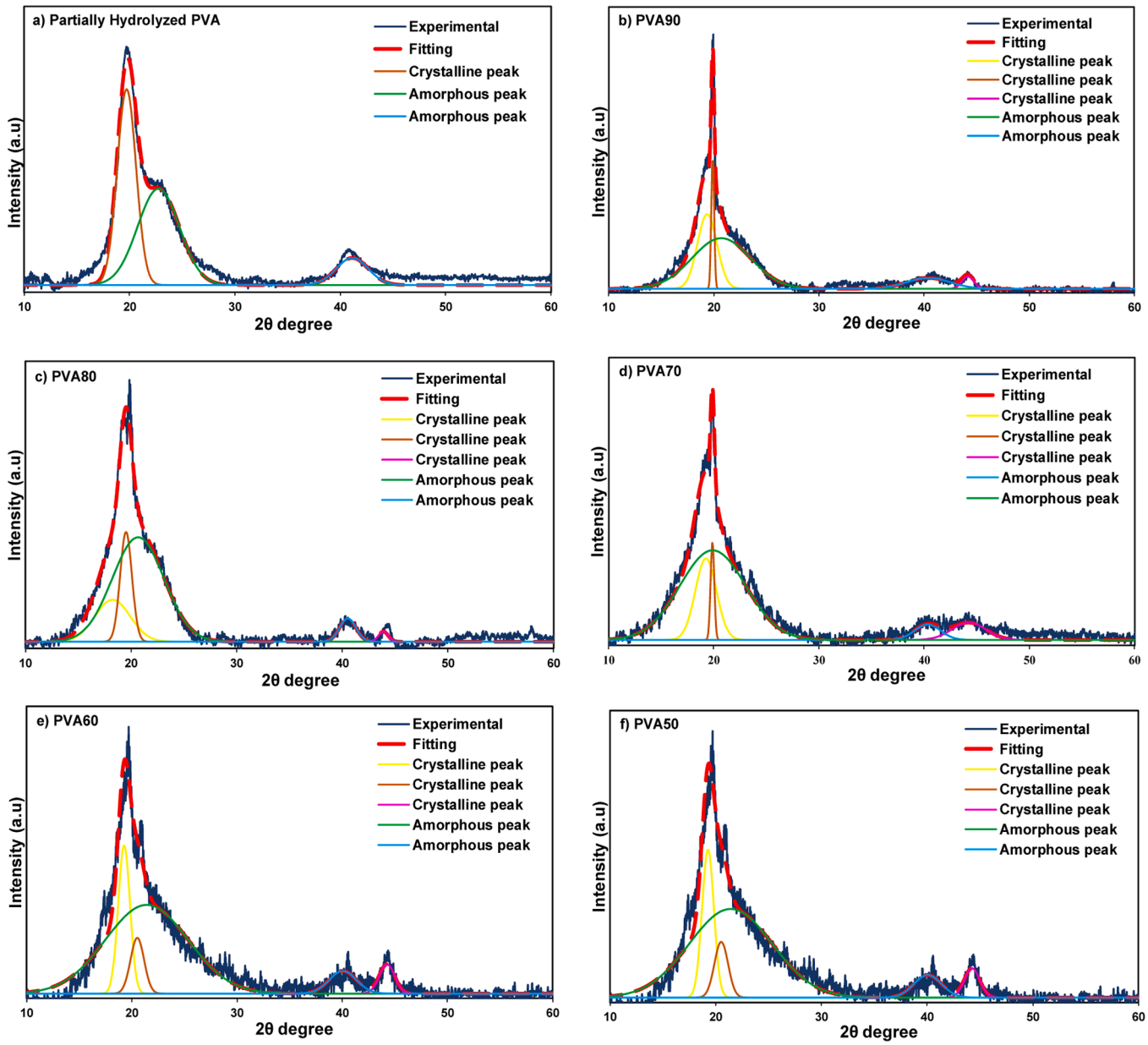

Fig. 11. Deconvoluted XRD spectra for (a) partially hydrolyzed PVA; (b) PVA90; (c) PVA80; (d) PVA70; (e) PVA60; (f) PVA50.

Table 8
The degree of crystallinity of various samples of SPE with different concentrations of salt.

Samples	Degree of Crystallinity (%)
Pure PVA	43.03
PVA90	36.65
PVA80	34.39
PVA70	29.85
PVA60	27.08
PVA50	30.74

The weight percentage for the pure salt starts to show constant weight percentage beyond 500 °C at around 45–50 % weight. For the partially hydrolyzed PVA, it experiences two major weight loss percentages 290 °C and 465 °C. At the first major weight loss (~290 °C), PVA undergoes a sudden decrease in weight caused by the creation of ether cross-links following the evaporation of water [51]. In addition, at this temperature, polyene formation may occur due to fast chain-stripping along the polymer backbone [52]. The second major weight loss (~465 °C) is caused by the continued degradation of the polymer's main structure, which can be attributed to the cleavage of the double bond in the polyenes. These polyenes, formed at lower temperatures previously, subsequently break down into single bonds and ultimately transform into aliphatic chains in this temperature [53].

There is an apparent decomposition at around 230–240 °C for both PVA90 and PVA60. The difference is that PVA90 shows a very high percentage weight loss in this region, while PVA60 only shows a steady but smaller weight loss percentage. This was a result of the intricate interaction between the PVA and $NaPF_6$ as previously examined in XRD and FTIR investigations. The formation of this complex raises the energy threshold needed to disrupt the temporary coordination, hence enhancing the thermal stability in this area. Beyond 400°C, both PVA90 and PVA60 show major degradation. The weight loss in this region is most likely due to the continuous decomposition of PVA and $NaPF_6$ in the SPEs [11]. The decomposition temperature at this region for PVA90 and PVA60 shows a drastic improvement (above 400 °C) compared to PVA100 or PVA powder (~300 °C). This means that after the addition of

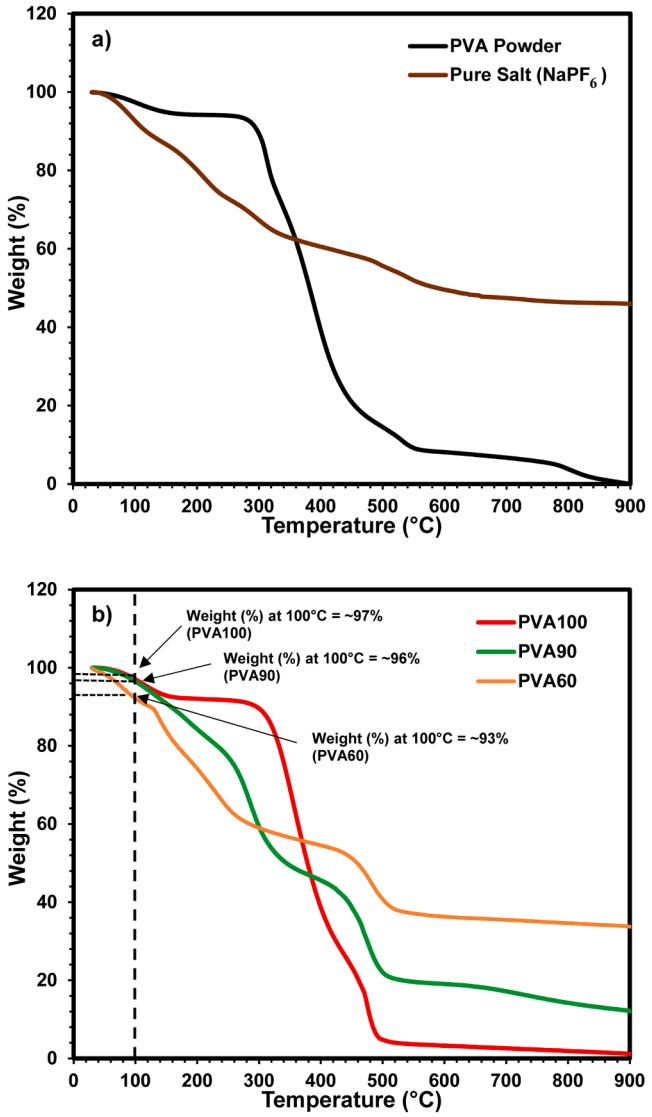

Fig. 12. The TGA curves for (a) partially hydrolyzed PVA powder and $NaPF_6$ salt; (b) PVA100, PVA90, and PVA60.

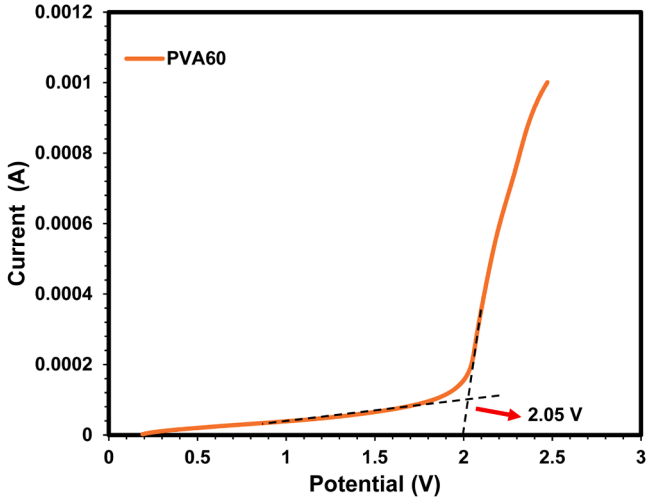

Fig. 13. The LSV curve for the highest conducting sample (PVA60) at room temperature.

salt, the thermal stability of the PVA-based SPE systems is greatly enhanced. In overall, it is observed that the PVA60 displays better thermal stability as decomposition that happens beyond the 400 °C temperature mark, PVA60 experienced weight loss at a higher temperature of ~450 °C compared to PVA90 with temperature of ~430 °C. This proved that the addition of salt does improve the thermal stability of this PVA-based SPE system.

3.10. LSV analysis

Linear sweep voltammetry (LSV) analysis is performed to investigate the electrochemical stability of the SPE, as well as to determine the electrolyte's maximum potential limit or the potential at which it begins to deteriorate. Fig. 13 shows the LSV plot for the SS|Highest Conducting Electrolyte (PVA60)|SS at 10 mV/s with the voltage range between 0 and 2.50 V. Note that the analysis was done at room temperature. The initial potential is seen to be swept toward more anodic values until the electrolyte experiences a sharp rise in current. A straight line was drawn in relation to the steady current and sudden current increase to determine the value of the decomposition voltage. In this case, the intersection point is the decomposition voltage which is 2.05 V. The value is enough for utilization in energy storage devices, where typically an electrolyte should have a breakdown voltage of at least 1.0 V [54]. The decomposition voltage obtained from this research is quite similar to the study by Brza et al. [55], where their PVA-based polymer electrolyte (PVA:NH_4SCN:Cd(II) plasticized with glycerol) reported the decomposition voltage or potential window of 2.10 V.

4. Conclusion

Free standing PVA-based SPEs with different concentrations of $NaPF_6$ are prepared using solution-casting method. The conductivity analysis using EIS shows that PVA60 exhibits an improved ionic conductivity of 3.65×10^{-5} S/cm from PVA90 with 2.13×10^{-9} S/cm. The temperature dependence study shows that the PVA-based SPEs obeys Arrhenius rules and the activation energy for all SPEs are calculated, where the activation energy for PVA60 recorded the lowest value of 0.149 eV. The highest conducting PVA-sample (PVA60) also exhibits the lowest relaxation time, as well as having the highest dielectric constant. It is also observed that if too much salt is added (PVA50), the ionic conductivity drops, while the activation energy and relaxation time increases. This is due to the presence of excess ions, which cannot be effectively incorporated into the polymer matrix, leading to an increased formation of ion pairs and aggregations in comparison to the free ions. The correlation between the AC conductivity and the movement of charge carriers was described by Jonscher's relation, and the frequency exponent (s) is determined. From that, the main goal of finding out the conduction model is achieved. The ion conduction mechanism is determined to adhere to the correlated barrier hopping (CBH) ion conduction model, where ions conduct through correlated hopping between sites by overcoming barrier heights or potential wells, with conductivity being dependent on both temperature and frequency. FTIR and XRD investigations were conducted to examine the formation of complexes between the host polymer and salt. According to the FTIR deconvolution, raising the $NaPF_6$ concentration increases the ion concentration (n) where PVA50 exhibits the highest ion number density. In the other hand, PVA60 exhibits the highest ion mobility (μ) and ion diffusion (D). The degree of crystallinity analyzed from the XRD data gives out information that the PVA60 has the lowest degree of crystallinity of 27.08 %. The TGA analysis shows that the addition of salt improved the thermal stability of the system. Lastly, the LSV analysis shows that the highest conducting sample has a suitable decomposition voltage and has good electrochemical stability. The findings of this study have verified that $NaPF_6$, when used as a conducting salt for electrolyte material, indicates a promising potential for usage in electrochemical storage devices.

CRediT authorship contribution statement

Jacky Yong: Writing – review & editing, Writing – original draft, Validation, Methodology, Investigation, Formal analysis, Data curation, Conceptualization. **Yung-Chung Chen:** Validation, Investigation. **Shujahadeen B. Aziz:** Validation, Supervision, Conceptualization. **Mayeen Uddin Khandaker:** Validation, Conceptualization. **Haw Jiunn Woo:** Writing – review & editing, Validation, Supervision, Project administration, Funding acquisition, Conceptualization.

Declaration of competing interest

The authors declare that they have no known competing financial interests or personal relationships that could have appeared to influence the work reported in this paper.

Acknowledgments

This work is supported by the Ministry of Higher Education of Malaysia for the Fundamental Research Grant (FRGS/1/2022/STG05/UM/02/3) awarded to Woo Haw Jiunn and University of Malaya research Grant (ST089-2022).

Data availability

No data was used for the research described in the article.

References

[1] G.Z. Chen, Supercapacitor and supercapattery as emerging electrochemical energy stores, Int. Mater. Rev. 62 (4) (2016) 173–202.
[2] S.B. Aziz, et al., Fabrication of high performance energy storage EDLC device from proton conducting methylcellulose: dextran polymer blend electrolytes, J. Mater. Res. Technol. 9 (2) (2020) 1137–1150, 2020/03/01/.
[3] R.I. Pushparaj, A.R. Kumar, G. Xu, Enhancing safety in lithium-ion batteries with additive-based liquid electrolytes: a critical review, J. Energy Storage 72 (2023) 108493, 2023/11/30/.
[4] S.B. Aziz, W.O. Karim, H.O. Ghareeb, The deficiency of chitosan:$AgNO_3$ polymer electrolyte incorporated with titanium dioxide filler for device fabrication and membrane separation technology, J. Mater. Res. Technol. 9 (3) (2020) 4692–4705, 2020/05/01/.
[5] V. St-Onge, M. Cui, S. Rochon, J.C. Daigle, J.P. Claverie, Reducing crystallinity in solid polymer electrolytes for lithium-metal batteries via statistical copolymerization, Commun. Mater. 2 (1) (2021) 83, 2021/08/03.
[6] M.H. Buraidah, L.P. Teo, S.R. Majid, A.K. Arof, Ionic conductivity by correlated barrier hopping in NH4I doped chitosan solid electrolyte, Phys. B Condens. Matter 404 (8) (2009) 1373–1379, 2009/05/01/.
[7] S.B. Aziz, Occurrence of electrical percolation threshold and observation of phase transition in chitosan(1−x):AgI x ($0.05 \leq x \leq 0.2$)-based ion-conducting solid polymer composites, Appl. Phys. A 122 (2016), 06/30.
[8] A. Asma, A. Rhaiem, K. Khirouni, K. Karoui, Synthesis, vibrational analysis, optical, ionic conductivity and conduction mechanism of γ-$NaCoPO_4$ compound, Res. Dev. Mater. Sci. 13 (2020), 04/17.
[9] M.H. Buraidah, A.K. Arof, Characterization of chitosan/PVA blended electrolyte doped with NH4I, J. Non Cryst. Solids 357 (16) (2011) 3261–3266, 2011/08/01/.
[10] O.G. Abdullah, S.B. Aziz, M.A. Rasheed, Structural and optical characterization of PVA:$KMnO_4$ based solid polymer electrolyte, Results Phys. 6 (2016) 1103–1108, 2016/01/01/.
[11] N. Farah, et al., Solid polymer electrolytes based on poly(vinyl alcohol) incorporated with sodium salt and ionic liquid for electrical double layer capacitor, Mater. Sci. Eng. B 251 (2019) 114468, 2019/12/01/.
[12] S.B. Aziz, M.A. Brza, M.H. Hamsan, M.F.Z. Kadir, S.K. Muzakir, R.T. Abdulwahid, Effect of ohmic-drop on electrochemical performance of EDLC fabricated from PVA:dextran:NH4I based polymer blend electrolytes, J. Mater. Res. Technol. 9 (3) (2020) 3734–3745, 2020/05/01/.
[13] C. Vaalma, D. Buchholz, M. Weil, S. Passerini, A cost and resource analysis of sodium-ion batteries, Nat. Rev. Mater. 3 (4) (2018) 18013, 2018/03/13.
[14] A.R. Nurohmah, et al., Sodium-ion battery from sea salt: a review, Mater. Renew. Sustain. Energy 11 (1) (2022) 71–89, 2022/04/01.
[15] D. Karabelli, et al., Sodium-based batteries: in search of the best compromise between sustainability and maximization of electric performance, Front. Energy Res. Rev. 8 (2020).
[16] Y. Zhang, et al., Sodium-ion capacitors: materials, mechanism, and challenges, ChemSusChem 13 (10) (2020) 2522–2539, 2020/05/22.
[17] P. Sj, A. Arya, A. Sharma, Selection of best composition of Na^+ ion conducting PEO-PEI blend solid polymer electrolyte based on structural, electrical, and dielectric spectroscopic analysis, Ionics 26 (2020) (Kiel)02/01.
[18] B J, K.K M A, M. Pillai, P. Vallachira, J. Sankaran, Development of a novel type of solid polymer electrolyte for solid state lithium battery applications based on lithium enriched poly (ethylene oxide) (PEO)/poly (vinyl pyrrolidone) (PVP) blend polymer, Electrochim. Acta 235 (2017), 03/01.
[19] Y. Zhu, J. Cao, H. Chen, Q. Yu, B. Li, High electrochemical stability of a 3D cross-linked network PEO@nano-SiO_2 composite polymer electrolyte for lithium metal batteries, J. Mater. Chem. A 7 (12) (2019) 6832–6839, https://doi.org/10.1039/C9TA00560A.
[20] M.H. Hamsan, M.F. Shukur, S.B. Aziz, Y.M. Yusof, M.F.Z. Kadir, Influence of NH4Br as an ionic source on the structural/electrical properties of dextran-based biopolymer electrolytes and EDLC application, Bull. Mater. Sci. 43 (1) (2019) 30, 2019/12/18.
[21] H.T. Ahmed, V.J. Jalal, D.A. Tahir, A.H. Mohamad, O.G. Abdullah, Effect of PEG as a plasticizer on the electrical and optical properties of polymer blend electrolyte MC-CH-LiBF4 based films, Results Phys. 15 (2019) 102735, 2019/12/01/.
[22] H. Bloom, E. Heymann, A.C.D. Rivett, The electric conductivity and the activation energy of ionic migration of molten salts and their mixtures, Proc. R. Soc. Lond. Ser. A Math. Phys. Sci/ 188 (1014) (1997) 392–414, 1997/01/01.
[23] K. Kondamareddy, R. Muchakayala, Y. Pavani, S. Bhavani, A.K. Sharma, V. Rao, Investigations on the effect of complexation of NaF salt with polymer blend (PEO/PVP) electrolytes on ionic conductivity and optical energy band gaps, Phys. B Condens. Matter 406 (2011) 1706–1712, 04/01.
[24] A. Arya, A. Sharma, Investigation on enhancement of electrical, dielectric and ion transport properties of nanoclay-based blend polymer nanocomposites, Polym. Bull. 77 (2020), 06/01.
[25] L. Porcarelli, C. Gerbaldi, F. Bella, J.R. Nair, Super soft all-ethylene oxide polymer electrolyte for safe all-solid lithium batteries, Sci. Rep. 6 (1) (2016) 19892, 2016/01/21.
[26] C. Cholant, et al., Study of the conductivity of solid polymeric electrolyte based on PVA/GA blend with addition of acetic acid, J. Solid State Electrochem. 24 (2020), 08/01.
[27] P. Singh, D.C. Bharati, H. Kumar, A. Saroj, Ion transport mechanism and dielectric relaxation behavior of PVA-Imidazolium ionic liquid based polymer electrolytes, Phys. Scr. 94 (2019), 10/01.
[28] M.A.M. Saeed, O.G. Abdullah, Effect of high ammonium salt concentration and temperature on the structure, morphology, and ionic conductivity of proton-conductor solid polymer electrolytes based PVA, Membranes 10 (10) (2024), https://doi.org/10.3390/membranes10100262.
[29] H.J. Woo, S.R. Majid, A.K. Arof, Dielectric properties and morphology of polymer electrolyte based on poly(ε-caprolactone) and ammonium thiocyanate, Mater. Chem. Phys. 134 (2) (2012) 755–761, 2012/06/15/.
[30] T. Selvi, M. Hema, Structural, thermal, vibrational, and electrochemical behavior of lithium ion conducting solid polymer electrolyte based on poly(vinyl alcohol)/poly(vinylidene fluoride) blend, Polym. Sci. Ser. A 58 (2016), 07/19.
[31] S.B. Aziz, M.F.Z. Kadir, M.H. Hamsan, H.J. Woo, M.A. Brza, Development of polymer blends based on PVA:POZ with low dielectric constant for microelectronic applications, Sci. Rep. 9 (1) (2019) 13163, 2019/09/11.
[32] H.J. Woo, S.R. Majid, A.K. Arof, Effect of ethylene carbonate on proton conducting polymer electrolyte based on poly(ε-caprolactone) (PCL), Solid State Ion. 252 (2013) 102–108, 2013/12/01/.
[33] J.O.M. Bockris, J.O.M. Bockris, A.K.N. Reddy, Modern Electrochemistry: Ionics, 1, Springer US, 1998.
[34] M.G. McLin, C.A. Angell, Ion-pairing effects on viscosity/conductance relations in Raman-characterized polymer electrolytes: lithium perchlorate and sodium triflate in PPG(4000), J. Phys. Chem. 95 (23) (1991) 9464–9469, 1991/11/01.
[35] K.P. Singh, P.N. Gupta, Study of dielectric relaxation in polymer electrolytes, Eur. Polym. J. 34 (7) (1998) 1023–1029, 1998/07/01/.
[36] S.Z. Yusof, H.J. Woo, A.K. Arof, Ion dynamics in methylcellulose–LiBOB solid polymer electrolytes, Ionics 22 (11) (2016) 2113–2121 (Kiel)2016/11/01.
[37] A.M. Farid, A.E. Bekheet, AC conductivity and dielectric properties of Sb2S3 films, Vacuum 59 (4) (2000) 932–939, 2000/12/01/.
[38] A. Chawla, A. Singh, M. Singh, P.S. Malhi, Small polaron hopping-assisted electrical conduction and relaxation in BCT and Mn-doped BCT samples, J. Asian Ceram. Soc. 7 (4) (2019) 558–568, 2019/10/02.
[39] O.G. Abdullah, R.R. Hanna, H.T. Ahmed, A.H. Mohamad, S.A. Saleem, M.A. M. Saeed, Conductivity and dielectric properties of lithium-ion biopolymer blend electrolyte based film, Results Phys. 24 (2021) 104135, 2021/05/01/.
[40] P. Bhargav, V. Madhu Mohan, A. Sharma, V. Rao, Investigations on electrical properties of (PVA:NaF) polymer electrolytes for electrochemical cell applications, Curr. Appl. Phys. 9 (2009) 165–171. CURR APPL PHYS01/31.
[41] I. Omkaram, R.P. Sreekanth Chakradhar, J.L. Rao, EPR, optical, infrared and Raman studies of VO^{2+} ions in polyvinylalcohol films, Phys. B Condens. Matter 388 (1) (2007) 318–325, 2007/01/15/.
[42] N. Ahad, E. Saion, E. Gharibshahi, Structural, thermal, and electrical properties of PVA-sodium salicylate solid composite polymer electrolyte, J. Nanomater. 2012 (2012), 08/16.
[43] M.A. Brza, et al., Characteristics of a plasticized PVA-based polymer electrolyte membrane and H^+ conductor for an electrical double-layer capacitor: structural, morphological, and ion transport properties, Membranes 11 (4) (2024), https://doi.org/10.3390/membranes11040296.
[44] Pritam, A. Arya, A.L. Sharma, Selection of best composition of Na+ ion conducting PEO-PEI blend solid polymer electrolyte based on structural, electrical, and dielectric spectroscopic analysis, Ionics 26 (2) (2020) 745–766 (Kiel)2020/02/01.
[45] A. Kumar, M. Madaan, A. Arya, S. Tanwar, A.L. Sharma, Ion transport, dielectric, and electrochemical properties of sodium ion-conducting polymer nanocomposite:

application in EDLC, J. Mater. Sci. Mater. Electron. 31 (13) (2020) 10873–10888, 2020/07/01.
[46] N.A. Shamsuri, S.N.A. Zaine, Y.M. Yusof, W.Z.N. Yahya, M.F. Shukur, Effect of ammonium thiocyanate on ionic conductivity and thermal properties of polyvinyl alcohol–methylcellulose–based polymer electrolytes, Ionics 26 (12) (2020) 6083–6093 (Kiel)2020/12/01.
[47] N.A.M. Noor, M.I.N. Isa, Investigation on transport and thermal studies of solid polymer electrolyte based on carboxymethyl cellulose doped ammonium thiocyanate for potential application in electrochemical devices, Int. J. Hydrog. Energy 44 (16) (2019) 8298–8306, 2019/03/29/.
[48] R. Ricciardi, F. Auriemma, C. De Rosa, F. Lauprêtre, X-ray diffraction analysis of poly(vinyl alcohol) hydrogels, obtained by freezing and thawing techniques, Macromolecules 37 (5) (2004) 1921–1927, 2004/03/01.
[49] F H, H.J. Woo, N. Aziz, m.z. Kufian, S.R. Majid, Synthesis of Al_2TiO_5 and its effect on the properties of chitosan-NH_4SCN polymer electrolytes, Ionics 19 (2013) 483–489 (Kiel)03/01.
[50] C.W. Liew, S. Ramesh, A.K. Arof, Characterization of ionic liquid added poly(vinyl alcohol)-based proton conducting polymer electrolytes and electrochemical studies on the supercapacitors, Int. J. Hydrog. Energy 40 (1) (2015) 852–862, 2015/01/05/.
[51] S. Kayal, R.V. Ramanujan, Doxorubicin loaded PVA coated iron oxide nanoparticles for targeted drug delivery, Mater. Sci. Eng. C 30 (3) (2010) 484–490, 2010/04/06/.
[52] A. Das, A.K. Thakur, K. Kumar, Evidence of low temperature relaxation and hopping in ion conducting polymer blend, Solid State Ion. 262 (2014) 815–820, 2014/09/01/.
[53] I. Stoševski, J. Krstić, N. Vokić, M. Radosavljević, Z.K. Popović, Š. Miljanić, Improved Poly(vinyl alcohol) (PVA) based matrix as a potential solid electrolyte for electrochemical energy conversion devices, obtained by gamma irradiation, Energy 90 (2015) 595–604, 2015/10/01/.
[54] S.B. Aziz, et al., Impedance, circuit simulation, transport properties and energy storage behavior of plasticized lithium ion conducting chitosan based polymer electrolytes, Polym. Test. 101 (2021) 107286, 2021/09/01/.
[55] M.A. Brza, et al., The study of EDLC device with high electrochemical performance fabricated from proton ion conducting PVA-based polymer composite electrolytes plasticized with glycerol, Polymers 12 (9) (2024), https://doi.org/10.3390/polym12091896 (Basel).